Point Sets Morphological Filtering and Semantic Spatial Configurations Modeling: application to microscopic image analysis

Nicolas Loménie, Daniel Racoceanu

Point Set Morphological Filtering and Semantic Spatial Configuration Modeling: application to microscopic image and bio-structure analysis

Nicolas Loménie*[1], Daniel Racoceanu[2]

Abstract

High-level spatial relation and configuration modeling issues are gaining momentum in the image analysis and pattern recognition fields. In particular, it is deemed important whenever one needs to mine high-content images or large scale image databases in a more expressive way than a purely statistically one. Continuing our previous efforts to incorporate structural analysis by developing specific efficient morphological tools performing on mesh representations like Delaunay triangulations, we propose to formalize spatial relation modeling techniques dedicated to unorganized point sets. We provide an original mesh lattice framework which is more convenient for structural representations of large image data by the means of interest point sets and their morphological analysis. The set of designed numerical operators is based on a specific dilation operator that makes it possible to handle concepts like "between" or "left of" over sparse representations of image data such as graphs. While basically proposing a new theoretical framework to reason about images, for the sake of illustration and discussion, we apply these new tools to high-level queries over large histopathological images which are, by nature, high-content and large size image data to be explored for clinical visual assessment.

Keywords: Shape analysis, mesh analysis, unorganized point set, spatial relation modeling, mathematical morphological operator, image exploration, graph representation, semantic query, visual reasoning, digital histopathology.

1. Introduction

Shape in computer vision usually refers to either an explicit segmented region over a radiometric image or an implicit feature vector as in Fig. 1. It is less commonly handled as a visual geometrical point set. Yet it has been long the traditional way to define synthetic object models in computer graphics. Recently, representations of virtual models as point sets have started to overtake the mainstream polygonal mesh or spline surface modeling due to both hardware considerations and a few theoretical advances [1].

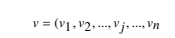

(a) (b) (c)

Figure 1: Shape as (a) a segmented subset of $\Re^2$; (b) a point set representation; (c) a feature vector $v \in \Re^n$.

On the other side of visual computing issues, traditional image analysis is facing all the more challenging issues as the size, resolution and pace of acquisition of images is exponentially growing, in particular in the satellite and medical fields generating huge amount of visual database to be processed. In that perspective, sparse handling of these data as opposed to redundant radiometric traditional coding schemes must be studied. Concise representations of images by the means of structural elements like edges, point sets or graphs of regions are picking up in the computer vision community [2, 3, 5, 6] and in particular in medical imaging applications [18, 34]. Geometrical representations like point sets for shape or pattern analysis are a means to smooth the way to the efficient handling of large radiometric images: First, geometric features are more stable than radiometric ones and second, as a global representation, they encompass more structural information than local radiometric patches do.

We are ultimately interested in extending usual image analysis tools to geometric representations such as perceptual graphs [4]. Beyond current mainstream works about statistical pattern recognition in the field of image analysis, roughly boiling down to a specific feature extraction step feeding supervised classification algorithms like support vector machines, the research works about structural representations of the image signal is gaining momentum even [2, 3] for the recognition of natural categories like horses. [5] proposed to use contour fragments as descriptors instead of radiometric patches and build a kind of structural codebook composed of the outer object contour fragments associated to their position with regard to the center

*Corresponding author
Email address: lomenie@mi.parisdescartes.fr (Nicolas Loménie*)
[1]CNRS - French National Center for Scientific Research
University Paris Descartes
CNRS UMI IPAL (I2R/A*STAR, NUS, UJF, IT, UPMC)
[2]CNRS - French National Center for Scientific Research
National University of Singapore
CNRS UMI IPAL (I2R/A*STAR, NUS, UJF, IT, UPMC)

of the object while [6] extended it to bring a major improvement to the representation by a coding (invariant to scale, translation and rotation) of the geometric properties of each group of k adjacent segments (kAS). One key point here is the definition of spatial arrangements of structural elements, and that proved to be useful even for natural images. The end-users can leverage spatial relation and configuration modeling to enhance the interactive mining process over high-content images or large scale image databases in a more expressive way than a purely statistically one [7]. In addition, this structural modeling is likely to be more resilient to radiometric variations inducing learning biases as well as more expressive for end-user interaction issues and, accordingly, to foster the capabilities of now well-studied and efficient statistical models using radiometric patches for instance [8].

In this paper, however, we are not directly dealing with object categorization but rather with spatial arrangement characterization by morphological considerations. In this perspective, we are considering the issue of high-level spatial relation representations. A few works have dealt with this issue concerning a kind of spatial reasoning in images from a structural point of view: that is how to model spatial relations like "between" or "around" in a sound and generic framework. [9], [10] and [11] provide good overviews or interesting ways for representing spatial relations in particular in the imprecise and uncertain universe of image analysis.

While most of the algorithmic solutions to this visual reasoning purpose operate either over usual dense radiometric images or within logical, abstract frameworks like first order logic, we propose here an original, theoretically sound and generic framework to work over sparse representations of visual scenes, such as graphs, in an operational way. This paper continues and in a sense completes our previous efforts for developing morphological tools for the analysis of point sets [12] and extends the seminal ideas about spatial relations modeling over sparse representations presented in [13]. In particular, this paper gives (a) a unified version of the mesh morphological operators (b) develops the set of spatial relationships modeling capabilities and (c) extends it to algorithmic fuzzy versions within a real bio-imaging application whereby the point set nuclei architecture plays a major role. Even though generic, we chose to closely relate this contribution to a specific application (that we are currently developing in the field of high-content histopathological image exploration and analysis) both for illustration and proof-of-concept purposes. In the following Section 2, we expose the medical context of spatial reasoning from an image analysis point of view with a few but inspiring related existing works specially highlighting the underlying nuclei architecture. Section 3 reviews the theoretical operators we designed for point set analysis and in particular the mathematical lattice framework. Then Section 4 presents the innovative contribution to the modeling of high-level linguistic spatial relation modeling over sparse representations of images as point sets. Last, Section 5 illustrates the handling of these spatial relationships within the medical application of interest while Section 6 draws significant theoretical and applicative perspectives of research in particular in the bio-imaging field.

2. Motivation in the Bio-imaging Context

When describing medical or biological images, it is not rare that high-level spatial descriptions be involved such as anatomical entities being "close to" or "left of" another one. In particular, a few works deal with anatomical descriptions based on macro image analysis [14–16]. Such qualitative reasoning capabilities should be as much as useful at a microscopic level. For instance, in [17], it is stated that there is suggestive evidence that directed localization of chromatin loci is one mechanism for regulating gene expression within the nucleus: inactivated chromosomes are predominantly located at the periphery of the nucleus, juxtaposed to the nuclear envelope, observing also an inverse correlation between proximity to the nuclear periphery and gene density. In the case of histo-pathological image analysis, not only the aspect but also the spatial configurations of biological entities are of major importance during the prognosis process. In Fig. 2, a sketch classification of spatial cell configurations is drawn for the prognosis of breast cancer from histo-pathological images.

(a)

(b)

Figure 2: (a) Theoretical spatial configuration of cells corresponding to various gradings and characteristics of breast cancer - Courtesy of `http://www.breastcancer.org`; (b) Mesh representations with nucleus seeds as vertices of α-complexes.

The automatic grading from such histo-pathological images remains a major scientific issue from both the computer and medical sciences sides. Physicians proceed by tedious, collaborative prognosis sessions involving visual description of Whole Slide Images (WSI) and hardly come to a rigorous consensus. The size of a WSI (around eight gigabytes of image data) constitutes by itself a technological barrier to handle the problem with the help of a computerized system. Any new tool enhancing the capabilities of browsing, focusing, exploring and thus mining such a huge digitalized image slide is valuable for the pathologists in order to perform the grading from numerical data.

The architecture of breast cancer relies on the spatial distribution of different biological entities such as nuclei, tubular formations or *lumina*, all of them to be detected in the image either by the pathologist or by the algorithm. Entails then a mental process of spatial reasoning about these entities and their organization that is not so much explicit because of the size of the slide. Thus, most grading procedures consist in looking at smaller image frames and scoring visual clues such as the size and the texture of cells as well as the homogeneity of the distribution of these attributes. But, much implicit knowledge involved in that procedure is related to reasoning about spatial relationships. For example, a pathologist will more likely search for mitoses in the periphery of invasive regions. From this statement, any improvement in the way pathologists can perform enriched spatial query in a digitalized slide can improve the quality of the grading. Besides, the basic biological

entity is the nucleus which is easier to extract with state-of-the-art image analysis tools than other biological entities. This is the reason why we consider the set of extracted nuclei as a useful, simplified representation of a slide on which the system can perform efficient spatial query. In addition, this simplified architectural/structural representation is required to handle such an amount of pixel data. Working on a restricted point set representation instead of the radiometric WSI downsizes this amount of data from around 2.5 billions radiometric color pixels up to 20 000 geometrical 2D points. In [18], the same kind of considerations gave rise to a successful attempt to adapt image processing frameworks (such as Partial Differential Equations based regularization methods) usually acting on radiometric images over a regular grid to unorganized point sets defined within graph representations. From now, the set of nuclei centroids can be seen as a set of geometrical unorganized point sets, that is a minimal structural representation of the architecture of the cell distribution in the tissue.

Thus, we do not work anymore on the regular lattices of radiometric images but on a new irregular lattice dedicated to geometric images. In previous recent works, [12] developed new morphological operators acting on meshes like Delaunay triangulations (see section 3). The combination of these operators made it possible to build sound and generic spatial relationships operators (see section 4). We added fuzzy representation capabilities including a new morphological operator acting on meshes and corresponding to the directional dilation as described in [19] for radiometric images. Then, we applied these new operators to the analysis and exploration of histopathological images in order to enhance the cognitive power of interaction between the pathologist and a prototyped virtual microscope (see section 5). Yet the designed framework is actually a new generic toolbox to handle structural representations of radiometric images as graphs of interest points. Last, as a proof-of-concept, we developed a Java interface[3] that implements most of the morphological operators acting on Delaunay triangulation described in this paper.

3. Point set and mesh morphological operators

In [12], we set up a formal extension to the topological mesh analysis proposed with the concepts of α-objects first exposed to define "what is the shape" of a point set in [21, 22]. So far, working on the shape analysis of unorganized point sets, we have developed new morphological operators dealing with mesh structures such as Delaunay triangulations in an efficient algorithmic way. In the following, our work can be illustrated as both point set analysis operators and mesh structure analysis operators depending on the nature of a specific value ϕ_T. Indeed, based on the same ranking operator *max* and *min* as α-objects use it, and directly related to the way mathematical morphology proceeds, we provided a sound algorithmic description of these morphological operators. Then, we proved that these algorithmic operators correspond to formal mathematical operators such as erosion or dilation. From that, we were able to design a set of useful filtering operators such as opening filters acting on point sets. We refer the interested reader to [12, 22] to get more details about topological considerations on the data structures and theoretical validation about these new dedicated operators. Nevertheless, for the paper to be self-contained, we give a different presentation (more compact and focused on the lattice framework [23, 24]) of these new operators in the following, insofar as, as noted by [25, 26], a very few works gave it a try to extend morphology to curved manifolds and to meshes and cell decompositions on curved manifolds ([27–31]).

3.1. Notations

Let us start with some notations about the geometrical and topological structures and then about the lattice framework.

Topological and geometrical structures. Let S be a point set in $\Re^2$. [22] details how to compute the spectrum of α-shapes $S_\alpha(S)$ for any visual point sets in 2D or 3D for any $\alpha \in [0, \infty[$ with: $S_\infty = conv(S)$, where *conv* stands for the convex hull, and $S_0 = S$ as limit cases.

Let us define k-simplices $\sigma_T = conv(T)$, $T \subseteq S$ and $|T| = k + 1$ for $0 \leq k \leq 2$. Let us remind that the α-objects rely on the Delaunay triangulation $Del(S)$ of S and the $\phi(T)$ values associated with any triangle $T \in Del(S)$, being the inverse radius of the circumscribe sphere to T in the framework of α-objects. Then, for the algorithmic design, we just need to remember that for each simplex $\sigma_T \in Del(S)$, there is a single interval so that σ_T is a face of the α-shape S_α, i.e. if, and only if, α is contained in this interval. Last, let $up(\sigma_T)$ be the set of all faces incident to σ_T whose dimension is one higher than that of σ_T, that is : $up(\sigma_T) = \{\sigma_{T'} \in Del \mid T \subset T' \text{ and } |T'| = |T| + 1\}$

Lattice structures. Let us now define some notations related to useful dedicated lattice structures.

For any point set $S \in \Re^2$, $\mathcal{M}(Del)$ is the set of meshes on $Del(S)$, i.e., the set of mappings from the triangles T in Del to ϕ_T values. As for now, T stands for any triangle in Del. A mesh $M \in \mathcal{M}(Del)$ is defined by $\{(T, \phi)\}_{T \in Del}$ or equivalently by a mapping $\phi : T \in Del \rightarrow [0, \infty[$.

$\wp(Del)$ is the set of all the corresponding sub-triangulations D_i of Del. From now, we can define two complete lattice structures for a point set including an order relation:

- the first one, within the set theory frame, called $\mathcal{L}_1 = (\wp(Del), \subseteq)$ where $D_1 \subseteq D_2$ denotes the relation : $\forall T \in Del, T \in D_1 \rightarrow T \in D_2$;
- the second one, within the functional theory frame, called $\mathcal{L}_2 = (\mathcal{M}(Del), \leq)$, where the partial ordering $\leq$ is defined by: $\forall M_1$ and $M_2 \in \mathcal{M}(Del), M_1 \leq M_2 \iff \forall T \in Del, \phi_T^1 \leq \phi_T^2$

3.2. α-objects and mesh lattices

Depending on the nature of the $\phi(T)$ values, the proposed operators correspond either to an extension of the α-objects concept for point sets or to new mathematical morphological operators acting on meshes. In the case of a $\phi(T)$ value related to

[3] To test the presented results, a Java application and its source code are available in the public domain at `http://www.sip-crip5.org/lomn/`.

Figure 3: A spectrum of $\alpha - objects$ derived from the Edelsbruner's modeling

intrinsic geometric properties of point set configurations such as the inverse radius of the circumsphere of the σ_T simplices, we can relate our operators to the α-objects concept that gives a set of operators to define and filter the shape of a point set. The operator α-bin defined later on in Equation 2 will make the connection between our operators and the $\alpha - objects$-based ones. If $\phi(T)$ is an extrinsic value (such as radiometric values associated to pixels on a regular grid) then our operators constitute new ways to process morphological properties over meshes.

Definition of α-objects. For each σ_T, two values λ_T and μ_T are derived :

$$\begin{cases} if\ |T| = 3, \lambda_T = \mu_T = \phi_T \\ else \begin{cases} \lambda_T = \min\{\lambda_{T'} | \sigma_{T'} \in up(\sigma_T)\} \\ \text{and} \\ \mu_T = \max\{\mu_{T'} | \sigma_{T'} \in up(\sigma_T)\} \end{cases} \end{cases}$$

Then we can compute three different topological kinds of α-objects spectra for planar graphs in 2D: α-shape, α-complex and α-Delaunay triangulations. Table 1 classifies the simplices of the Delaunay triangulation $Del(S)$ in order to compute these various topological/geometrical structures:

$$\begin{aligned} C_\alpha &= \{\text{Singular } \sigma_T\} \cup \{\text{Regular } \sigma_T\} \cup \{\text{Interior } \sigma_T\} \\ Del_\alpha &= \{\text{Interior Triangles T}\} \cup \{\sigma_T \in \partial T\} \\ \partial S_\alpha &= \{\text{Regular } \sigma_T\} \end{aligned} \quad (1)$$

where ∂ stands for the boundary of a structure.

Note that $Del_\infty(S) = Del(S)$ and $S_\alpha = |C_\alpha| = |Del_\alpha|$. We chose to represent the shape of a point set by the triangulation of its inner region, thus, introducing new α-objects called Del_α. Doing that, we put apart any topological issues related to singular σ_T.

Table 1: Obtaining α-objects.

σ_T is...	Singular	Regular	Interior
Triangle			$\alpha \in [\phi_T, \infty[$
Edge, $\notin \partial conv(S)$	$\alpha \in [\phi_T, \lambda_T[$	$\alpha \in [\lambda_T, \mu_T[$	$\alpha \in [\mu_T, \infty[$
$\in \partial conv(S)$	$\alpha \in [\phi_T, \lambda_T[$	$\alpha \in [\lambda_T, \infty[$	
Vertex, $\notin \partial conv(S)$	$\alpha \in [0, \lambda_T[$	$\alpha \in [\lambda_T, \mu_T[$	$\alpha \in [\mu_T, \infty[$
$\in \partial conv(S)$	$\alpha \in [0, \lambda_T[$	$\alpha \in [\lambda_T, \infty[$	

Point set and mesh binarization. Let us also define the binarization operator α-bin as follows :

$$\forall M \in \mathcal{M}(Del(S)), \alpha\text{-bin}(M) = \{T \in Del(S) \mid \phi_T > \alpha\} \quad (2)$$

and thus,

$$|\alpha\text{-bin(M)}| = |\alpha\text{-Del}(S)| = |\alpha\text{-shape(S)}| \quad (3)$$

In particular when ϕ_T is the inverse radius of the circumsphere of T we get the spectrum of α-region describing the shape of a point set S and we can state that an α-shape(S) is related to a kind of binarization operators acting on spaces whose structure is given by an unorganized point set S (note that here again we do not handle any topological issues about singular simplices).

Based on the lattice structure, the binarization of a point set is defined by:

$$\forall S \in \mathfrak{R}^2, \alpha\text{-bin}(S) = \{x \in S \mid T \in Del(S)\ and\ \phi_T > \alpha_{opt}\} \quad (4)$$

with

$$\alpha_{opt} = 2 * \text{median}_{T \in Del(S)}(\alpha) \quad (5)$$

By extension and based on the organic relation between S and $Del(S)$ in terms of neighborhood and topology, we can write α-bin(S) $\equiv$ α-bin(M) when $M = \{T \in Del(S), 1/\rho_T\}$.

Point set and mesh morphological operators.

To define morphological operators, we need to affect to each triangle values e_T and d_T in addition to the measure ϕ_T, defined by :

$$\begin{aligned} \mathrm{e}_T &= \min\{\phi_{T'} | T' \in \nu(T)\} \\ \mathrm{d}_T &= \max\{\phi_{T'} | T' \in \nu(T)\} \end{aligned} \quad (6)$$

where $\nu(T)$ (in the framework of α-objects) is the set of all triangles T of Del sharing at least one vertex with the triangle T, that is:

$$\nu(T) = \{T' \in Del | T' \cap T \neq \emptyset\} \quad (7)$$

In our case, ν_T plays the role of a structuring entity (element or graph [27]). We proved in [12] that with this definition of a structuring entity the following designed operators are actual mathematical dilation and erosion.

Indeed, in the framework of α-objects, we define the α-eroded of any point set as the reunion of all the triangles of Del_α whose e_T value is superior to α, that is :

$$\alpha\text{-eroded}(S) = \{T' \in Del | e_{T'} > \alpha\} \quad (8)$$

(a) (b)

Figure 4: (a) A point set S in $\mathfrak{R}^2$; (b) α-eroded(S) for $\alpha = \alpha_{opt}$

And in a dual way, the α-dilated of any point set is defined as the reunion of all the triangles of Del_α whose d_T value is superior to α, that is :

$$\alpha\text{-dilated}(S) = \{T' \in Del | d_{T'} > \alpha\} \quad (9)$$

Then, in the lattice framework, we define two operators e(M) and d(M) on the complete lattice $\mathcal{L}_2$ by :

$$\forall M \in \mathcal{M}(Del),$$
$$\mathrm{e}(M) = \{T \in Del, e_T\} \text{ and } \mathrm{d}(M) = \{T \in Del, d_T\}$$

(a) (b)

Figure 5: (a) A point set S in $\Re^2$; (b) α-dilated(S) for $\alpha = \alpha_{opt}$

with e_T and d_T defined in Eq. 6.

From this point on, $e^{\mathcal{L}_1}$ and $e^{\mathcal{L}_2}$ denote the erosions defined on $\mathcal{L}_1$ and $\mathcal{L}_2$, respectively. Last, we defined more formally the erosion and dilation operators on the sub-triangulation complete lattice $\mathcal{L}_1$. Let D be a sub-triangulation of Del. Let D be seen as a subset of the topological space Del. Then, T is an interior triangle of D (that is $T \in int(D)$) if there exists a neighborhood of T which is contained in D. Then, with this formal definition $T \in int(D) \equiv \exists\, \nu(T) \subset D$:

$$\begin{aligned} &\forall M \in \wp(Del), \\ &\qquad \mathrm{e}(D) \;=\; \{T \in Del \mid T \in int(D)\} \\ &\qquad \mathrm{d}(D) \;=\; \{T \in Del \mid T \notin int(D)^C\} \end{aligned} \tag{10}$$

We proved that $e(D)$ and $d(D)$ are respectively erosion and dilation morphological operators on $\mathcal{L}_1$.

Last, we stated the following:

$$\begin{aligned} &\forall M \in \mathcal{M}(Del(S)), \\ &\alpha\text{-bin}(e^{\mathcal{L}_2}(M)) = e^{\mathcal{L}_1}(\alpha\text{-bin}(M)) = \alpha\text{-eroded}(S) \\ &\alpha\text{-bin}(d^{\mathcal{L}_2}(M)) = d^{\mathcal{L}_1}(\alpha\text{-bin}(M)) = \alpha\text{-dilated}(S) \end{aligned} \tag{11}$$

showing with Eq. (4) that our new structures and operators can embed the α-objects concept in a lattice framework, regardless topological issues due to singular σ_T in the simplicial complex structures. That is, computing the eroded and dilated sub- triangulations as defined previously is equivalent to first computing the α-complex and performing the erosion and dilation directly in that geometrical structure.

The interesting point is that with these lattice structures, we inherit all the properties of classical morphology and particularly for the opening and closing filtering operators.

3.3. Mesh Morphological Filtering: a new tool

We have established so far that a spectrum of filtered shape extracted out of any point set can be computed extending the spectrum of classical α-objects first proposed in [22]. We highlighted the fact that depending on the nature of the ϕ_T values associated to the simplicial complex extracted from S we get structures directly related to visual shape representation of a point set like in the framework of α-object or we get new operators acting on meshes whose vertices are the sites in S.

From now, we need to adapt these new tools for a practical use in the case of spatial relationship representation between entities defined over a Delaunay triangulation $Del(S)$ of a point set S.

As for now, ϕ_T values are limited to the interval $[0, 1]$ and is related to a notion of visibility of the triangle or of membership to an object of interest within the mesh. Thus, we can define interactively or automatically sub-triangulations of interest as regions of interest in the meshed image. In the following, we illustrate our results on the histopathological image in Fig. 6(a) and its corresponding underlying meshed nuclei architecture. This image is about 1000 x 1000 pixels size and each pixel is $0.25\mu m$ resolution. The Whole Slide Image contains hundreds of such sample images. In Fig. 6(b), we illustrate the definition of a region of interest over $Del(S)$ by a set of triangles whose ϕ_T values are set to 1 (in white) and others to 0 (no filling color).

(a) (b)

Figure 6: (a) A real biological image and the underlying nuclei architecture embedded in a Delaunay triangulation $Del(S)$ mesh representation; (b) a crisp region of interest as a sub-triangulation of $Del(S)$: A membership function of 1 is represented by a white triangle and a membership of 0 is represented by transparent triangles.

In that case, the binarization performed by the previously defined operator α-bin on $Del(S)$ is made by another process either interactively by an end-user or automatically by any image analysis process. The notion of α cut or α spectrum is no longer needed. We will focus now on operational morphological operators defined on the lattice $\mathcal{L}_2 = (\mathcal{M}(Del), \leq)$ where the mapping ϕ_T is restricted to $[0, 1]$ with a fuzzy interpretation in term of membership function to a region of interest.

Thus, we can define the whole set of operators in a more classical way similar to regular grid formulation used with radiometric images. The structuring entity is the neighborhood $\nu(T)$ associated to each triangle whose definition can vary according to a specific relevant morphological operator (see Section 4). Having proved that the operators designed to obtain these new structures are theoretically sound as mathematical adjunctions, they can provide the whole set of mathematical morphological operators like opening acting on an unorganized point set S or on a mesh M. We can define opening $\mathrm{o}(M)$ end closing $\mathrm{c}(M)$:

$$\forall M \in \mathcal{M}(Del(S)),\ \mathrm{o}(M) = \mathrm{d} \circ \mathrm{e}(M) \textit{ and } \mathrm{c}(M) = \mathrm{e} \circ \mathrm{d}(M) \tag{12}$$

In functional radiometric mathematical morphology, an opening is idempotent but the size of the structuring element is flexible. To adapt the size of the structuring element in the case of mesh operators, we need to define opening of order n as:

$$\forall M \in \mathcal{M}(Del(S)),\ \mathrm{o}^n(M) = \mathrm{d}^n \circ \mathrm{e}^n(M) \tag{13}$$

so that:

$$\forall n > 1,\ \mathrm{o}^n(M) \neq \mathrm{o}(M) \tag{14}$$

but we still get the idempotent property of the mathematical morphology opening:

$$\forall M \in \mathcal{M}(Del(S)) \textit{ and } \forall n \in \mathbb{N}, (\mathrm{d} \circ \mathrm{e}(M))^n = \mathrm{d} \circ \mathrm{e}(M). \tag{15}$$

(a) (b)

Figure 7: (a) A point set S in $\Re^2$; (b) α-open(S) for $\alpha = \alpha_{opt}$

and benefits of all the inherited operators based on the erosion and the involution operators ^{c}:

$$\forall M \in \mathcal{M}(Del(S)), M^c = \{T \in Del, 1 - \phi_T\} \tag{16}$$

Thus, as expected,

$$\forall M \in \mathcal{M}(Del(S)), \mathrm{e}(M) = \mathrm{d}(M^c)^c \quad (17)$$

The proof of the theoretical soundness of these operators is directly related to the lattice structure presented in [12] and briefly in the previous subsection. Then, we can deal with new ways of expressing spatial relationships with fuzzy extent over mesh representations like Delaunay triangulations and illustrate how it can benefit the interactive exploration of huge images as the domain of histopathological biopsy images provides.

Extension to fuzzy neighborhood. Let us focus on the dilation operator. A definition of a fuzzy dilation in the functional framework is given by (see [32]):

$$D_\nu(\mu)(x) = sup_y t[\mu(y), \nu(x-y)] \quad (18)$$

where μ design the fuzzy set to be dilated, ν the structuring element, x and y points of space and t any $t-norm$ (see [33]). Usual $t-norms$ are given by: $t(a,b) = min(a,b)$ or the Lukasiewicz' definition $t(a,b) = max(0, a+b-1) \forall (a,b) \in [0,1]$. With that latter $t-norm$ definition in mind, we propose hereby an algorithmic formulation convenient for the computation of such a fuzzy dilation over an irregular discretized space. Let us define a maximum order of dilation N for the fuzzy dilation. This is related to the shape of a fuzzy structuring element in classical mathematical morphology. We define a fuzzy discrete neighborhood on meshes and a specific $t-norm$ formulation in the case of mesh dilation that makes it possible to compute the fuzzy dilation $d^f(M)$ of a mesh M within the lattice $\mathcal{L}_2$ by Algorithm 1.

Algorithm 1 Fuzzy Dilation

INPUT: a mesh M defined over the lattice $\mathcal{L}_2$
for all $i = 0$ to $N+1$ **do**
  for all $T \in Del$ **do**
    $d_T = 0$;
    $d_T = \max\{d_T, \max_{T' \ominus \nu(T)} \{(\phi_T, \phi_{T'} + (1 - i/N) - 1\}\}$;
  end for
  for all $T \in Del$ **do**
    $\phi_T = d_T$;
  end for
end for
OUTPUT a resulting mesh $d^f(M)$

The fuzzy structuring element or neighborhood is defined in an algorithmic way and can be represented by the discrete membership function along a neighborhood order as illustrated in Fig. 8(a).

At this point, it is worth noting that defining morphological operators on irregular grids is not as straightforward as often stated [20]. The flexibility of defining versatile structuring elements has not been really handled in a tractable way so far in the world of general graphs [27]. Likewise the definition of sound fuzzy sets over these representations has not been theoretically dealt with. These seminal, practical tools give first insights into the development of morphological operators acting on meshes in 2D as well as in 3D.

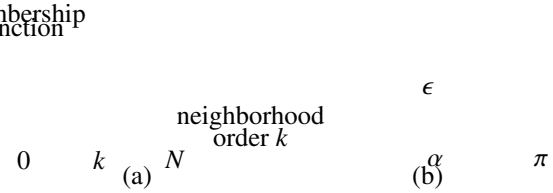

Figure 8: (a) Discrete membership function along a neighborhood order; (b) Crisp angle representation for the directional dilation.

4. Mesh Morphological Operators and Spatial Relationships

In the field of pure image analysis, few works have dealt with the effective modeling of spatial relations such as "between", "surround" or "along". The major difficulty comes from the high level of contextual references associated to the semantic of these linguistic representation of image content. Obviously, inherent issues about accurate, robust segmentation of the region of interests within the image are part of the difficulties to handle such a tough problem in comparison with artificial intelligence approaches. For instance, the notion of crisp adjacency that is central to most of the formal system dealing with spatial reasoning is error-prone due to imprecise segmentation results. To us, the more interesting modeling results in the field of image processing can be found in [19] for which, besides the use of mathematical morphology operators, a fuzziness representation framework deals with imprecision and context-dependent numerical implementations of such symbolical descriptions.

Our aim is to apply similar considerations to geometrical representations. Usually, Delaunay triangulations can be associated with the underlying point-of-interests architecture associated with a radiometric image. We state that these simplified representations are more correlated with the semantic of the images and hence consider that spatial relation reasoning on such representations should be closer to the cognitive spatial reasoning processing performed by the pathologists onto histopathological images, and more generally by linguistic-based query.

We developed a Java interface as a plugin for the *imageJ* platform to test the proposed operators that implements all the morphological operators acting on Delaunay triangulation described hereby. We added fuzzy representation capabilities included a new morphological operator acting on meshes and corresponding to the directional dilation as described in [19] for radiometric images.

4.1. The directional dilation

The whole set of spatial relation concepts modeling is based on the directional dilation operator defined over regular lattice images. We propose a specific operator for directional dilation over sparse representations such as Delaunay triangulations.

Let α be the directional angle with regard to the horizontal axis of the representation plane. For any mesh $M \in \mathcal{L}_2$, the definition of the neighborhood $\nu(T)$ of a mesh triangle T acts as a directional structural element of direction α:

$$\nu_\alpha(T) = \{T' \in Del | T' \cap T \neq \emptyset \, and \, \angle(T, T') < \alpha + \epsilon\} \quad (19)$$

with

$$\angle(T, T') = \angle(\overrightarrow{B_T B_{T'}}, (\overrightarrow{Ox})) \quad (20)$$

where B_T is the barycenter of the triangle T.

Eq. 19 defines an anisotropic neighborhood referred as ν_α, to be put in parallel with the isotropic neighborhood definition $\nu_{iso}(T) = \nu(T)$ of Eq. 7, where *iso* stands for isotropic as opposed to directional and α stands for the angle with the horizontal axis $(\overrightarrow{Ox})$ and ϵ is the width or tolerance angle of the structuring element (see Fig. 8(b)).

We can define the directional dilation as:

$$\forall M \in \mathcal{M}(Del(S)), \mathrm{d}_{\alpha,\epsilon}(M) = \mathrm{d}_{\nu_\alpha}(M) \quad (21)$$

where d_ν stands for the computation of d_T values over a specific system of neighborhood ν. When ϵ is not written, $\epsilon = \pi/8.0$ and $d_{\alpha,\epsilon} = d_\alpha$.

It is worthwhile being able to define fuzzy appreciations of such qualitative concepts as spatial relations that depend both on the context and on the reference object. This is the reason why we designed a fuzzy version for all the morphological operators acting on meshes following the algorithmic procedure in Alg. 1. The left fuzzy operator is directly obtained by combining Equation 21 associated with the directional neighborhood ν_α into the algorithmic procedure used to compute d^f.

4.2. The basic relations "left of" and "around"

Directional relations can now be defined. For instance, the absolute directional spatial relation like "left of" is defined as follows:

$$\mathrm{Left}_{dil}(M_1) = \mathrm{d}^n_\pi(M_1) \; with \; n/\, \mathrm{d}^n_\pi(M_1) = \mathrm{d}^{n+1}_\pi(M_1) \quad (22)$$

where d^n stands for $\mathrm{d} \circ \mathrm{d} \circ ... \circ \mathrm{d}$ *n times*.

Fig. 9 illustrates the region "left of" of the biological *lumina* region M_1 as defined in Fig. 6(b). The region $\mathrm{Left}_{dil}(M_1)$ in 9(a) corresponds to the left landscape defined over an irregular grid. Due to this irregularity, the output region need to be post-processed with a opening-like mesh filtering or at least in this case a dilation one. The final filtered region $\mathrm{d}_{\nu_{iso}}(\mathrm{Left}_{dil}(M_1))$ is presented in 9(b) with holes filled up. In general, any semantic region obtained by the mesh operator needs to be post-processed with an opening-like operator in order to provide compact region to the linguistic queries.

(a)

(b)

Figure 9: (a) The left region of the region M_1 in Fig 6; (b) The filtered open region left of M_1 with ν_{iso} : $\mathrm{d}_{\nu_{iso}}(\mathrm{Left}_{dil}(M_1))$.

The fuzzy version of the left dilation operator is illustrated in Fig. 10 in which the dilation operator d^n_π is replaced by its algorithmic fuzzy version defined in Alg. 1 in which the neighborhood structuring element ν is replaced by ν_π:

$$\mathrm{Left}^f_{dil}(M_1) = \mathrm{d}^f_\pi(M_1) \quad (23)$$

(a)

(b)

Figure 10: (a) The fuzzy left region of the region M_1; (b) The resulting mesh after an isotropic opening.

Similarly, we can also define a fuzzy spatial relation like "around" as illustrated in Fig. 11:

$$\mathrm{Around}_{fuzDil}(M_1) = \mathrm{d}^f_{\nu_{iso}}(M_1) \quad (24)$$

ans its post-processed version with an mesh opening $o(Around_{fuzDil}(M_1) = d^f_{\nu_{iso}}(M_1))$ as described respectively in Fig. 11(a) and (b).

(a) (b)

Figure 11: (a) The fuzzy region 'around M_1'; (b) The filtered open region around M_1.

4.3. The complex relation "between"

As for now, we can consider the more complex and subjective spatial relation like "between". We refer the reader to [19] for the thorough presentation of the modeling issues about this very high-level concept, taking into account the extent of the different reference objects. We define here new morphological operators giving the region "between" of two spatial mesh entities M_1 and M_2 defined over $\mathcal{L}_2$. We refer again to three possible definitions of this relation based on directional dilations as reviewed in [19]:

$$\beta_{dil}(M_1, M_2) = d^n[d^n(M_1) \cap d^n(M_2)] \cap M_1^C \cap M_2^C \quad with \quad n = inf\{k / d^k(M_1) \cap d^k(M_2) \neq \emptyset\}$$

$$\beta^1_\alpha(M_1, M_2) = d^n_\alpha(M_1) \cap d^n_{\pi+\alpha}(M_2) \cap M_1^C \cap M_2^C \quad (25)$$

$$\beta^2_\alpha(M_1, M_2) = d_\alpha(M_1) \cap d_{\pi+\alpha}(M_2) \cap M_1^C \cap M_2^C \cap [d_\alpha(M_1) \cap d_\alpha(M_2)]^C \cap [d_{\pi+\alpha}(M_1) \cap d_{\pi+\alpha}(M_2)]^C$$

Fig. 12 and Fig. 13 illustrate the different steps of the morphological processing of the underlying mesh associated with the studied histopathological image for two regions of interest with the definition β_{Dil} and β^1_α respectively. We based our result on a crisp dilation operator. In case of a fuzzy definition, we replace the mathematical operator d by the algorithmic operator d^f and the $\cap$ operator is a t-norm defined over the mesh lattice by:

$$\forall M_1, M_2 \in \mathcal{M}(Del(S)),$$
$$t(M_1, M_2) = \{T \in Del(S), t(\phi_T^1, \phi_T^2)\} \quad (26)$$

with $t(\phi_T^1, \phi_T^2)$ a t-norm on the real lattice such as $t(a, b) = min(a, b)$.

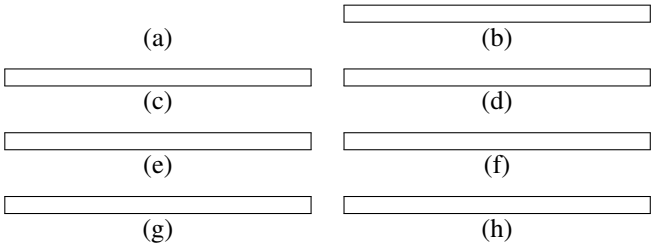

Figure 12: (a) Two sub-meshes of interest M_1 and M_2; (b) The dilated meshes (b) $\mathrm{d}_{(}^2 M_1$) and (c) $\mathrm{d}_{(}^2 M_2$); (d) Their intersection $\mathrm{d}^2(M_1) \cap \mathrm{d}^2(M_2)$; (e) and the twice dilated of the intersection $\mathrm{d}^2[\mathrm{d}^2(M_1) \cap \mathrm{d}^2(M_2)]$; (f) The complemented mesh $M_1^C \cap M_2^C$; (g) and the final output of the between region operator $\beta_{Dil}(M_1, M_2)$ as defined in Equation **??**; (h) the filtered result after an isotropic opening $\mathrm{o}(\beta_{Dil}(M_1, M_2))$.

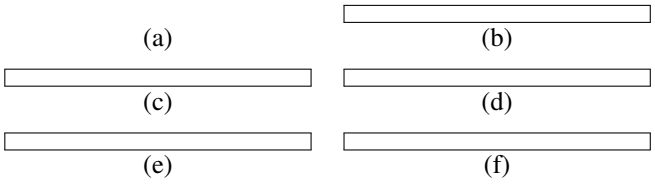

Figure 13: (a) Two sub-meshes of interest M_1 and M_2; (b) The twice dilated meshes $\mathrm{d}_\alpha^n(M_1)$ and (c) $\mathrm{d}_{\pi+\alpha}^n(M_2)$; (d) The intersection $M_1^C \cap M_2^C$; (e) the region between $\beta_\alpha^1(M_1, M_2)$ as defined in Equation 25; (f) after an isotropic opening filtering $\mathrm{o}(\beta_\alpha^1(M_1, M_2))$.

Due to the non-regular pavage of the underlying topological space, a post-filtering step by an isotropic opening filter is required to obtain coherent results (see Fig. 12(g)). If the second region of interest is not convex, as illustrated in Fig. 14, the third definition gives better results removing parts in the concavity.

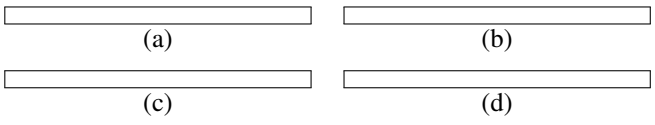

Figure 14: (a) One non convex sub-mesh of interest M_2; (b) Result with the second definition $\beta_\alpha^1(M_1, M_2)$; (c) $[\mathrm{d}_\alpha(M_1) \cap \mathrm{d}_\alpha(M_2)]^C \cap [\mathrm{d}_{\pi+\alpha}(M_1) \cap \mathrm{d}_{\pi+\alpha}(M_2)]^C$; (d) Result with the third definition $\beta_\alpha^2(M_1, M_2)$.

In general, the choice of the angle α should incorporate much information about the extent of the different objects of reference. In this study, we choose the average angle between pairs of respective triangles $T_1 \in M_1$ and $T_2 \in M_2$. Note also that the tolerance angle is set quite large to 22.5 degrees to smooth the results to the irregular pavage of the 2D space (see section 5 for more discussion about that specific issue).

4.4. High-level query

With the specific morphological framework defined over meshes, we are able to define high-level semantic queries over a mesh representation of objects of interest by combining different operators via $t-norm$ when conjunctions of properties occur or $t-conorm$ (like the max operator that stands also for the set operator $\cup$) when disjunctions of properties occur ([33]). For example, we can express the query what is the region "near and left" the region $M_1$by the following operator:

$$\mathrm{NearLeft}(M_1) = t(\mathrm{Around}_{fuzDil}(M_1), \mathrm{o}_{\nu_{iso}}(\mathrm{Left}_{dil}(M_1))) \quad (27)$$

with t a t-norm defined over the mesh lattice (see Eq. 26). Fig. 15 illustrates the result on the biological image.

Figure 15: The left and near region $t(\mathrm{Around}_{FuzDil}(M_1), \mathrm{o}_{\nu_{iso}}(\mathrm{Left}_{Dil}(M_1)))$.

5. Applications and discussion

All these functionalities can be very useful whereby one needs to reason about spatial entities corresponding to unorganized point sets as in the case of extracted nuclei from medical images (see [34] for interesting statistical analysis of nuclei architecture structures embedded in a mesh representation for breast cancer diagnosis). Seminal works tried to apply similar structural analysis of tissue images based on Delaunay graphs representations few years ago [35, 36] but have not been pushed forward so far. This is what we propose in the following in particular for digitized histopathology which is a brand new challenge in the field of bio-imaging as digital mammograms used to be over the last two decades.

5.1. Spatial relation concepts

As for now, we can answer the two types of questions raised by spatial reasoning:

- which is the region of space corresponding to a spatial query about a reference object M_i ? and, if necessary, what is the fuzzy mesh description of this region ?
- to which degree an object O belongs to that region ?

In comparison to the seminal works in [19], we can answer these questions with specific tools over a mesh representation that is on an irregular pavage of the space corresponding to the informative structural part within the image and not on the classical regular pavage over radiometric images. We remind the reader the importance of such a simplified representation in the case of high content image or large image data like new satellite or microscopic imaging devices provide from now on in a breakthrough way. These representations should be more efficient that classical radiometric, redundant by nature, images and its related processing algorithms not tractable for now over large amount of data due to computational and storage constraints.

In the previous section, we illustrated with numerous examples the numerical nature of answers our operators "around", "left of", "between' can reach to the first type of questions, possibly with a fuzzy description of these meshed resulting regions. In this section, we go further in the description of the operator outcomes from the end-user interaction point of view ending up with a discussion about the efficiency of such a sparse modeling of spatial relations. Fig. 16 illustrates the regions corresponding to the fuzzy version of the *Between* operator $\beta^f_\alpha(M_1, M_2)$ for the regions M_1 and M_2 and then the region between M_1 M_2 and M_3 can be obtained by combination of such operators such as:

$$\text{Between}(M1, M2, M3) = \bigcup_{k=1,2,3} \beta^f_\alpha(\beta^f_\gamma(M_i, M_j), M_k) \qquad (28)$$

as Fig. 16(c)(d) illustrates it for $\beta^f_\alpha(\beta^f_\gamma(M_1, M_2), M_3)$.

(a) (b)

(c) (d)

Figure 16: (a) Three meshed regions of interest M_1, M_2 and M_3; (b) the region between M_1 and M_2 $\beta^f_\alpha(M_1, M_2)$; (c) $\beta^f_\gamma(\beta^f_\alpha(M_1, M_2), M_3)$; (d) with the three regions superimposed in transparency.

In Fig. 17 we illustrate a level set for the fuzzy operator "around" for the inner region of interest M_3. The topology and density underlying the biological image is taken into account in contrast to the mere notion of iso-density distance usually used for radiometric morphological image operators.

(a) (b)

(c) (d)

(e) (f)

Figure 17: (a) Fuzzy meshed region M_a "around" the central region M_3; (b) the opening of this region $o(M_a)$; (c) in transparency over the biological image; (d) the binarized Delaunay triangulation $M_b = \alpha\text{-bin}(Del(S))$; (e) $M_f = M_b \cap \text{o}(M_a)$; (f) $\alpha\text{-bin}(ProximityLevelSet \cap M_f)$.

That simplified representation based on the natural architecture of the image is of major importance with the new imaging devices providing such high-content, large image data at very high rate. For the sake of illustration, in our histopathological application, Tab. 2 gives an idea of the amount of data to be processed by either the clinician or the numerical system. Then, Fig. 18 illustrates the level of details depending of the acquisition resolution. Note that the images at each of the listed resolution must be stored for clinical and virtual microscopy purposes. Note that the sample in Fig. 18(b) is a 1024 x 1280 pixels sample image at a resolution x40 out of over 2000 such samples tiling the global image slide.

Last, these morphological operators can be applied as it is to perform structural analyses of different nuclei architecture of breast cancer. In Fig. 19, the classification of the sketched cases

Table 2: Histopathological images data.

	Size (pixels)	Size (bytes)
x1	1 018 x 768	3.05 Mo
x10	3 664 x 2 763	39.54 Mo
x20	14 657 x 11 054	632.48 Mo
x40	58 630 x 44 216	7.77 Go

(a)

(b)

Figure 18: (a) Whole Slide Image at resolution x1; (b) Sample image at resolution x40 out of over 2000 samples tiling the WSI.

of various types of breast cancer architectures can be achieved by morphological and topological analyses of the underlying meshes. For the sake of illustration, we present below how with very basic morphological operators on such kinds of geometrical architectures we can discriminate at a high-level of description between various kinds of breast cancer configurations. In Figure 19, a morphological analysis based on both the α-complex and an opening filtering of the underlying Delaunay triangulations Del_α of the set of nuclei centroids can lead to an effective discrimination of these differently graded histopathological breast cancer drawings, by the means of compared structural features such as the number of connected components or the Euler characteristics related to the topology of the mesh and in particular to the number of holes or connected components in the structure (see Table 3). For instance, the Euler number EN of a surface is easily computed from the mesh representation as $EN = F - E + V$ where F is the number of faces, E the number of edges and V the number of vertexes. Note that this number can be related to the number of connected components minus the number of holes. In a way, global implicit spatial relations are processed in this example making it possible to exhibit a digital encoding of the bio-structure similar to the DNA or chromosomal representation in evolutionary algorithms paradigm. In the following, beyond these meaningful topological considerations, we will focus on more explicit spatial relation representations.

Table 3: Geometric criteria to discriminate between various cancer types computed on $M_1 - o^2(M_1)$ (see Fig. 19(c)). Median Size of 0 refers to small size and 1 to large size. EN, CC and MS stands respectively for Euler Number, number of Connected Components and σ^2-simplex Median Size whose concatenation provide a digital structural coding of the observed bio-structure.

Cancer type	EN	CC	MS
Normal cells	1	1	1
Ductal hyperplasia	0	1	0
Atypical ductal	1	1	0
DCIS	0	0	0
DCIS-MI	2	2	0
Invasive	5	5	0

(a) (b) (c)

Figure 19: The nuclei architecture and on the left (a) $Del_{\alpha_{opt}}$ representation; (b) in the middle, opening of order 2 $o^2(Del_{\alpha_{opt}})$ as an opening based morphological filtering; (c) at right, the difference between $Del_{\alpha_{opt}}$ and $o^2(Del_{\alpha_{opt}})$. Combining topological and morphological measures such as the number of connected components, the Euler number, the median face size between these various representations makes it possible to discriminate between the various levels of pathological spatial organizations.

In particular, the Ductal Carcinoma In Situ, rather difficult to discriminate automatically by statistical means because it is a highly versatile structure in shape and size, is characterized by a certain topological and morphological stability to opening filtering (compare column 1 and 2) in comparison to other type of architectures. Also, the invasive and the micro-invasive cases can be discriminated by a thorough analysis of the third column exhibiting more connected components for the invasive case. Of course, experiments on real images have been carried and showed that more structural and morphological criteria involved in automatic procedures provide efficient way to discriminate such spatial configurations and all the more from an human-computer interface point of view. For instance, Fig. 20 illustrates how to use the morphological operators interactively by the end-user (physician or automatic microscope) to focus on region of interests for breast cancer analysis: diagnosis or acquisition process. The resulting mesh is obtained as $o^2(Del_\alpha(S)) \cap Del_\alpha(S)$. The point sites are obtained by a basic image analysis procedure combining wavelet analysis, binarization and sampling on a 3072 x 3072 pixels sub-image taken out of the Whole Slide Image at resolution x40 whose global size is over 200 times bigger.

(a)

(b)

(c)

(d)

Figure 20: (a) 3072x3072 pixels size sub-image of a Whole Slide Histopathological Image; (b) The corresponding site points S; (c) $Del_\alpha(S)$; (d) Focusing on regions of interest $o^2(Del_\alpha(S)) \cap Del_\alpha(S)$.

5.2. Semantic concepts

Last, by setting the parameter ϕ_T to a measure of the size of triangles rather than a measure of the shape as the circumsphere characterizes, Fig. 21 illustrates how, with minimal interactions, it is possible to decompose the biological images of size 1024 x 1024 (top right quadrant of the previous image in Fig. 20) into meaningful biological elements like Ductal Carcinoma In Situ alike or normal cells by the means of morphological operators.

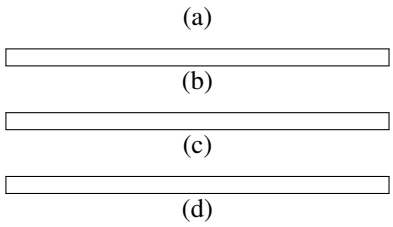

Figure 21: (a) 1024x1024 pixels size sub-image of a Histopathological WSI; (b) $Del_\alpha(S)$; (c) Focusing on DCIS alike areas with the $o^2(Del_\alpha(S))$ mesh filtering; (d) Focusing on normal cells areas with the $Del_\alpha(S) \cap (o^2(Del_\alpha(S)) \cap Del_\alpha(S))^c$ mesh filtering operator.

In Fig. 22, we discriminate between real tubule formation and DCIS configuration images based on the structural analysis described in Fig. 19. The tubule formation corresponds to the normal cell configuration except that it does not correspond to a real duct, rather to a natural organization of cells in the tissue. Basically, a high representation of such spatial configuration is a clue of healthy breast tissue in histopathology.

(a) (b) (c)

(d) (e) (f)

Figure 22: On the left (a) $Del_{\alpha_{opt}}$ representation of a tubular bio-structure; (d) of a DCIS bio-structure. In the middle, opening of order two $o^2(Del_{\alpha_{opt}})$ as an opening based morphological filtering of (b) the tubular formation; (e) the DCIS formation. At right, the difference between $Del_{\alpha_{opt}}$ and $o^2(Del_{\alpha_{opt}})$ for the (c) tubular formation and (d) the DCIS formation.

Furthermore, by nature, this set of techniques is quite resilient to low-level image extraction artifacts as illustrated in Fig. 23. In this experiment, only the epithelial cells are detected in Fig. 23(a) and some cell artifacts are detected in Fig. 23(d). The morphological analysis of the point set is robust to this shape noise for the detection of In Situ cases.

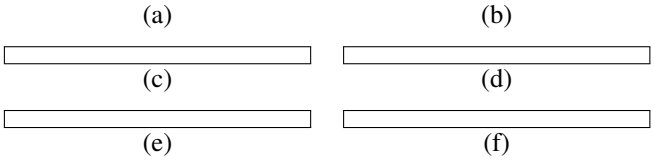

Figure 23: (a) Point set extracted without artifact, M; (b) and with artifacts, M_{noise}; (c) Binarization of M; (d) Binarization of M_{noise}; (e) Opening of M (f) Opening of M_{noise}.

6. Conclusion

To sum up, based on original mathematical morphological filters dedicated to unorganized point sets, we developed new

generic operators to perform structural analysis of images via an architectural representation as mesh of interest points for instance. In particular, a new way for handling spatial relation queries has been proposed and illustrations over histopathological images proved the usefulness of this new framework to interactively explore huge images. Beyond the applicative aspect, these operators have been proved to be theoretically sound from the mathematical lattice framework side. Accordingly, these tools open new ways to anchor high-level semantic and spatial relation concepts in the field of image analysis. In perspective, a thorough analysis of topological aspects about the extension to a lattice of simplicial complexes including the edges and the vertices in the morphological process as attempted in [37, 38] should raise interesting new theoretical issues for mathematical modeling and powerful computerized representations for topological study and understanding of biological processes.

7. References

[1] Zwicker, M., Pauly, M., Knoll, O., Gross, M. Pointshop 3D: An Interactive System for Point-Based Surface Editing. SIGGRAPH (2002).

[2] Lafarge, F., Gimel'farb, G., Descombes, X. Geometric Feature Extraction by a Multimarked Point Process. IEEE Trans. Pattern Analysis and Machine Intelligence, 32 (9) (2010) 1597-1609.

[3] Felzenszwalb, P.F., Girshick, R.B., McAllester, D., Ramanan, D., Object Detection with Discriminatively Trained Part-Based Models, IEEE Transactions on Pattern Analysis and Machine Intelligence, 32 (9) (2010) 1627 - 45.

[4] F. Meyer, Skeletons and perceptual graphs, Signal Processing, 16 (4) (1989) 335 - 363.

[5] J. Shotton, A. Blake, R. Cipolla, Multi-Scale Categorical Object Recognition Using Contour Fragments, IEEE Trans. Pattern Analysis and Machine Intelligence, 30 (7) (2008) 1270-1281.

[6] V. Ferrari, L. Fevrier, F. Jurie, C. Schmid, Groups of Adjacent Contour Segments for Object Detection, IEEE Trans. Pattern Analysis and Machine Intelligence 30 (1) (2008) 36-51.

[7] Y. Liu, Zhang, D., Lu, G., Ma, W.-Y., A survey of content-based image retrieval with high-level semantics, Pattern Recognition, 40 (1) (2007) 262-282.

[8] Brown, M., Gang Hua, Winder, S., Discriminative Learning of Local Image Descriptors, EEE Trans. Pattern Analysis and Machine Intelligence 33 (1) (2011) 43-57.

[9] E. Clementini, P. Di Felice, Approximate Topological Relations, International Journal of Approximate Reasoning (16) (1997) 173-204.

[10] S. Winter, Uncertain Topological Relations between Imprecise Regions, International Journal of Geographical Information Science 14, (5) (2000) 411- 430.

[11] P. Matsakis, L. Wendling, A new way to represent the relative position between real objects, IEEE Transactions on Pattern Analysis and Machine Intelligence 21 (7) (1999) 634-643.

[12] N. Lomenie, G. Stamon, Morphological Mesh filtering and alpha-objects, Pattern Recognition Letters 29 (10) (2008), 1571-1579.

[13] N. Lomenie, D. Racoceanu, Spatial relationships over sparse representations, in: IEEE Image and Vision Computing, Wellington, New Zealand, 2009.

[14] O. Colliot, 0. Camara, I. Bloch, Integration of Fuzzy Spatial Relations in Deformable Models - Application to Brain MRI Segmentation, Pattern Recognition (8) (2006) 1401-1414.

[15] Gianni, D., McKeever, S., Yu, T., Britten, R. and Delingette, H., Sharing and reusing cardiovascular anatomical models over the Web: a step towards the implementation of the virtual physiological human project, Philosophical Transactions of The Royal Society A, 368 2010) 3039-56.

[16] Mechouche, A., Morandi, X., Golbreich, C. and Gibaud, B., A hybrid system using symbolic and numeric knowledge for the semantic annotation of sulco-gyral anatomy in brain MRI images, IEEE Transactions on Medical Imaging, 28 (8) (2009) 1165-78.

[17] R. Swedlow, Nuclear dynamics: where genes are and how they got there, Genome Biology 2 (3) (2001).

[18] V.T. Ta, O. Lezoray, A. Elmoataz, S. Schupp, Graph-based Tools for Microscopic Cellular Image Segmentation, Pattern Recognition, Special Issue on Digital Image Processing and Pattern Recognition Techniques for the Detection of Cancer 42 (6) (2009) 1113-25.

[19] I. Bloch, O. Colliot, R.M. Cesar, On the ternary spatial relation "between", IEEE Trans. on Systems, Man, and Cybernetics, Part B: Cybernetics 36 (2) (2006) 312-327.

[20] Chaussard, J., Couprie M. and Talbot H. (2010), Robust skeletonization using the discrete lambda-medial axis, *Pattern Recognition Letters*, doi:10.1016/j.patrec.2010.09.002

[21] H. Edelsbrunner, D.G. Kirkpatrick, On the shape of set of points in the plane, IEEE Trans. on Information Theory (29) (1983) 551-559.

[22] H. Edelsbrunner, E.P. Mucke, E.P., Three-dimensionnal alpha-shapes, ACM Transactions on Graphics 13 (1) (1994) 43-72.

[23] H. Heijmans, C. Ronse, The algebraic basis of mathematical morphology I: dilations and erosions, Computer Vision, Graphics, & Image Processing 50 (3) (1990) 245-295.

[24] J. Serra, Image Analysis and Mathematical Morphology, Volume 2: theoretical advances, London Academic Press, 1988.

[25] M. Peternell, H. Pottmann, T. Steiner, Hough Transform and Laguerre Geometry for the Recognition and Reconstruction of Special 3D Shapes, Research Report, Institute of Discrete Mathematics and Geometry, Vienna, Austria, 2003.

[26] H. Pottmann, T. Steiner, M. Hofer, C. Haider, A. Hanbury, The Isophotic Metric and Its Application to Feature Sensitive Morphology, in: Computer Sciences Springer, Lecture Notes (ed), European Conference on Computer Vision (ECCV'04), vol. 3024, (2004) 560-572.

[27] H. Heijmans, P. Nacken, A. Toet, L. Vincent, Graph Morphology, Journal of Visual Communication and Image Representation 3 (1) (1992) 24-38.

[28] J. Roerdink, Mathematical morphology on the sphere, in: SPIE Conf. Visual Communications and Image Processing, (1990) 263-271.

[29] J. Roerdink, Manifold Shape : from differential geometry to mathematical morphology, in : Shape in Picture, Springer-Verlag, 1994.

[30] C. Rossl, L Kobbelt, H.P. Seidel, Extraction of feature lines on triangulated surfaces using morphological operators, in: Smart Graphics, AAAI Spring Symposium, 2000.

[31] L. Vincent, Graphs and Mathematical Morphology, Signal Processing 16 (4) (1989) 365-388.

[32] I. Bloch, H. Maitre, Fuzzy mathematical morphologies: A comparative study, Pattern Recognition 28 (9) (1995) 1341-1387.

[33] D. Dubois, H. Prade, Fuzzy sets and systems: Theory and Applications, New York: Academic, 1980.

[34] S. Doyle, S. Agner, A. Madabhushi, M. Feldman, J. Tomaszewski, Automated Grading of Breast Cancer Histopathology Using Spectral Clustering with Textural and Architectural Image Features, in: 5th IEEE International Symposium on Biomedical Imaging: From Nano to Macro, ISBI, (2008) 496-499.

[35] Della Mea, V. and Beltrami, C. Analysis of the spatial arrangement of cells in the proliferative breast lesions. Lecture Notes in Computer Science, Image Analysis and Processing, 974 (1995) 247-252.

[36] Della Mea, V., Finato, N. and Beltrami, C. A graph-based approach to the structural analysis of proliferative breast lesions. Lecture Notes in Computer Science, Artificial Intelligence in Medicine, 934 (1995) 413-414.

[37] J. Cousty, L. Najman, J. Serra, Some morphological operators in graph spaces, in: Computer Sciences Springer, Lecture Notes

(ed), Mathematical Morphology and Its Application to Signal and Image Processing, vol. 5720 (2009) 149-160.

[38] R. Levillain, T. Géraud, L. Najman, Milena: Write Generic Morphological Algorithms Once, Run on Many Kinds of Images, in: Computer Sciences Springer, Lecture Notes (ed), Mathematical Morphology and Its Application to Signal and Image Processing, vol. 5720, (2009) 295-306.